

in changing environments and compared against a set of baselines.

The paper is structured as follows: Section II surveys the related work and Section III introduces the problem, and the collision avoidance constraint. Section IV details CIAO alongside some considerations on feasibility, safety and practical challenges. In Section V we detail how CIAO can be used for trajectory optimization and RHC. The experiments and results are discussed in Section VI. A summary and an outlook is given in Section VII.

II. RELATED WORK

Trajectory optimization methods try to find time-optimal and collision-free robot trajectories by formulating and solving an optimization problem [1]–[11], [13], [14], [17]. Classical approaches to obstacle avoidance include [18]–[22]. These approaches do neither produce optimal trajectories, nor unify planning and control, nor account for complex robot dynamics.

Another simple and effective method that is still used in practice is the elastic-band algorithm [13]. The computed paths, however, are generally non-smooth, i.e. they are not guaranteed to satisfy kinodynamic constraints, nor does this algorithm compute a velocity profile. Like Zhu et al. [7], our approach aims to fix this shortcoming while building up on the notion of (circular) free regions. Instead of optimizing velocity profile and path length separately, as done in [7], [13], we optimize them jointly utilizing a model predictive control (MPC) setup. Also the authors in [17] provide an approach which combines elastic-band with an optimization algorithm. Contrarily to ours, their approach does not enforce obstacle avoidance as constraint, and requires a further controller for trajectory tracking.

Also [11] proposes RHC to unify trajectory optimization and tracking, but their approach does not include a strategy for obstacle avoidance. In [11] an unconstrained nonlinear program (NLP) is solved online, while CIAO is solving a constrained NLP online, that enforces collision freedom as constraint.

Nowadays optimization based methods receive increasingly more attention. Popular methods include CHOMP [2], TrajOpt [3], OBICA [5], and GuSTO [6], which have been shown to produce smooth trajectories efficiently. They typically use a simplified system model to compute a path from the current to the goal state (or set), and further need an additional controller to steer the system along the pre-computed path. The proposed method, CIAO, is MPC-based and provides algorithms for both trajectory optimization and RHC, simultaneously controlling the robot and optimizing its trajectory.

Frasch et al. [8] propose an MPC with box-constraints to model obstacles and road boundaries. Liniger et al. [9] handle obstacles in a similar way, but apply contouring control, i.e. the approach steers a race car in a corridor around a predefined path. These frameworks do not consider arbitrarily placed obstacles, particularly no moving obstacles, which makes them unsuitable for many applications. In our approach we handle more complex obstacle definitions, modeled according to a generic nonlinear and nonconvex distance

function. To this end, we propose a novel constraint formulation which is shown to be a convex inner approximation of the actual collision avoidance constraint. Herbert et al. [4] propose a hybrid approach to safely avoid dynamic obstacles. In this work, the trajectory tracker does not consider the obstacles explicitly, but relies on the planning layer. On the contrary, our method presents a unified approach for all robot motion planning, control, and obstacle avoidance, using constrained, nonlinear MPC.

The recently proposed method GuSTO [6], like several other common algorithms, e.g. [3], [8], [9], [17], uses sequential convex programming (SCP). This requires a complete convexification of the originally nonlinear and nonconvex trajectory optimization problem. This is accomplished by linearizing the system dynamics (or kinematics) and incorporating paths constraints, including collision avoidance, as penalties in the objective function. In general these approximations may lead to infeasible, i.e. colliding or kinodynamically intractable trajectories, and typically several SCP iterations are required to find a feasible solution. CIAO, on the other hand, solves partially convexified NLPs, using a convex inner approximation of the collision avoidance constraint, and finds feasible solutions in fewer iterations, typically one. The individual iterations are computationally cheaper and feasibility is preserved. Since the dynamical model is accounted for by the NLP-solver, linearization errors are minimized. Finally CIAO can be considered as a trust region method [23], where the nonlinear state constraints are approximated with a convex inner approximation.

III. PROBLEM FORMULATION

We approach the problem of finding a kinodynamically feasible, collision free trajectory by formulating and solving a constrained OCP. Kinodynamic feasibility is ensured by using a dynamical model to simulate the robot's behavior and collision avoidance is achieved constraining the robot to positions with a *minimum distance* \underline{d} to all obstacles.

The set of all points in the the robot's *workspace* $\mathcal{W} \subseteq \mathbb{R}^n$ that are occupied by obstacles is called the *occupied set* \mathcal{O} . The Euclidean distance to the closest obstacle for any position in the workspace, i.e. $\mathbf{p} \in \mathcal{W}$, is given by the *distance function* $d_{\mathcal{O}} : \mathcal{W} \rightarrow \mathbb{R}$:

$$d_{\mathcal{O}}(\mathbf{p}) = d(\mathbf{p}; \mathcal{O}) = \min_{\mathbf{o} \in \mathcal{O}} \|\mathbf{p} - \mathbf{o}\|_2. \quad (1)$$

To ensure convergence of Alg.1 we require that it is bounded, i.e. $\exists \bar{d} > 0$ such that $d_{\mathcal{O}}(\mathbf{p}) \leq \bar{d} \forall \mathbf{p} \in \mathcal{W}$. The area for which $0 < d_{\mathcal{O}}(\mathbf{p}) < \underline{d}$ holds is called the *safety margin*.

We can now formulate the obstacle avoidance constraint by requesting that the Euclidean distance between the robot's position $\mathbf{p} \in \mathcal{W}$ and any element of \mathcal{O} has to be larger or equal to \underline{d} . As shown in Lem. 1 we can write it compactly using the distance function.

Lemma 1: Let \mathcal{O} be the occupied set, $\underline{d} > 0$ be a safety distance and $d_{\mathcal{O}}$ be the distance function as defined in (1). Then $d_{\mathcal{O}}(\mathbf{p}) \geq \underline{d}$ is equivalent to $\|\mathbf{p} - \mathbf{o}\|_2 \geq \underline{d} \forall \mathbf{o} \in \mathcal{O}$.

Proof: This follows directly from the distance function's definition in (1). ■

Remark: A point $\mathbf{p} \in \mathcal{W}$ that satisfies $d_{\mathcal{O}}(\mathbf{p}) \leq \underline{d}$ is called 'free'. To ensure that only 'free' points satisfy Lem. 1, the

minimum distance \underline{d} has to be chosen > 0 . Therefore we assume $\underline{d} > 0$ to be fixed from now on.

We can now formulate an OCP that enforces collision avoidance as path constraint:

$$\begin{aligned} \min_{\mathbf{x}(\cdot), \mathbf{u}(\cdot)} \quad & \int_0^T l(\mathbf{x}(t), \mathbf{u}(t), \mathbf{r}(t)) dt + l_T(\mathbf{x}(T), \mathbf{r}(T)) \\ \text{s.t.} \quad & \mathbf{x}(0) = \bar{\mathbf{x}}_0, \\ & \mathbf{x}(T) \in \mathbb{X}_T, \\ & \dot{\mathbf{x}}(t) = f(\mathbf{x}(t), \mathbf{u}(t)), \quad t \in [0, T], \\ & h(\mathbf{x}(t), \mathbf{u}(t)) \leq 0, \quad t \in [0, T], \\ & d_{\mathcal{O}}(\mathbf{p}(t)) \geq \underline{d}, \quad t \in [0, T], \end{aligned} \quad (2)$$

where $\mathbf{x}(\cdot) : \mathbb{R} \rightarrow \mathbb{R}^{n_x}$ denotes the robot's state, $\mathbf{u}(\cdot) : \mathbb{R} \rightarrow \mathbb{R}^{n_u}$ is the vector of controls, $\mathbf{r}(\cdot) : \mathbb{R} \rightarrow \mathbb{R}^{n_x+n_u}$ provides reference states and controls, T is the length of the MPC horizon in seconds, the function $l(\cdot)$ denotes the cost at time point t and $l_T(\cdot)$ the terminal cost, $\bar{\mathbf{x}}_0$ is robot's current state, and $\mathbb{X}_T \subseteq \mathbb{R}^{n_x}$ is the set of admissible terminal states. We use the common shorthand $\dot{\mathbf{x}}$ to denote the derivative with respect to time, i.e. $\dot{\mathbf{x}} = \frac{\partial \mathbf{x}}{\partial t}$. The function f is the dynamic model of the system, the function h implements a set of path constraints, e.g. physical limitations of the system, and $\mathbf{p}(t) = S_{\mathbf{p}} \cdot \mathbf{x}(t) \in \mathcal{W}$ denotes the robot's pose in the workspace with a selector matrix $S_{\mathbf{p}}$ chosen accordingly.

IV. CONVEX INNER APPROXIMATION (CIAO)

In this section we describe how we solve the OCP presented in (2) by adopting a convex inner approximation of the actual distance function constraint presented in Sec. III.

First we discretize (2) using a direct multiple shooting scheme as proposed by [16]. The resulting NLP is a function of \mathbf{r} , $\bar{\mathbf{x}}_0$, and the sampling time Δt . Using the shorthand $\mathbf{x}_k = \mathbf{x}(k \cdot \Delta t)$, $k \in \mathbb{Z}$ for cleaner notation, we discretize (2) as:

$$\min_{\mathbf{w}} \quad J(\mathbf{w}, \mathbf{r}) \quad (3a)$$

$$\text{s.t.} \quad \mathbf{x}_0 - \bar{\mathbf{x}}_0 = 0, \quad (3b)$$

$$\mathbf{x}_N \in \mathbb{X}_T, \quad (3c)$$

$$\mathbf{x}_{k+1} - F(\mathbf{x}_k, \mathbf{u}_k; \Delta t) = 0, \quad k = 0, \dots, N-1, \quad (3d)$$

$$h(\mathbf{x}_k, \mathbf{u}_k) \leq 0, \quad k = 0, \dots, N, \quad (3e)$$

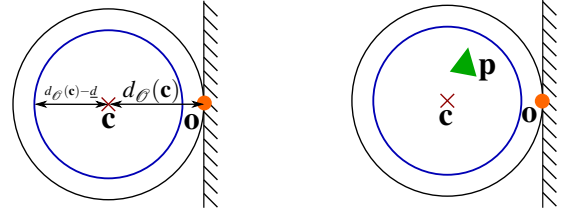
$$d_{\mathcal{O}}(\mathbf{p}_k) \geq \underline{d}, \quad k = 0, \dots, N, \quad (3f)$$

where $\mathbf{w} = [\mathbf{x}_0^\top, \mathbf{u}_0^\top, \dots, \mathbf{u}_{N-1}^\top, \mathbf{x}_N^\top]^\top \in \mathbb{R}^{n_w}$ a vector of optimization variables that contains the stacked controls and states for all N steps in the horizon, similarly \mathbf{r} contains the reference states and controls, $J(\mathbf{w}, \mathbf{r}) = \sum_{k=0}^{N-1} l(\mathbf{x}_k, \mathbf{u}_k, \mathbf{r}_k) + l_T(\mathbf{x}_N, \mathbf{r}_N)$ is the discretized objective function, with stage cost l_k and terminal cost l_N , and F models the discretized system dynamics for the given sampling time Δt . The feasible set of this problem (3) is denoted by $\mathcal{F}_{(3)} \subset \mathbb{R}^{n_w}$.

We now detail modifications to the NLP (3) above, namely the proposed convex inner approximation of (3f).

A. Free Balls: A Convex Inner Approximation of the Obstacle Avoidance Constraint

The actual obstacle avoidance constraint formulated in Lem. 1 is generally nonconvex and nonlinear, which makes it



(a) Example of a free ball around the center \mathbf{c} marked by the red cross for a 2D environment. It is also the center of the circles, the black circle has radius $d_{\mathcal{O}}(\mathbf{c})$, and the blue circle radius $d_{\mathcal{O}}(\mathbf{c}) - \underline{d}$.

(b) Example for free ball constraint. The green arrow head depicts the robot's current position \mathbf{p} , the orange dot the closest obstacle \mathbf{o} , the circles, and the red cross are identical to the ones in 2a.

Fig. 2: The left figure illustrates the free ball concept, the right shows how it can be used as a constraint.

ill-suited for rapid optimization. We propose a convex inner approximation of the constraint that is based on the notion of free balls (FBs), as proposed in [13] and extended by [7]. For cleaner notation we first define the *free set*.

Definition 1: Let \mathcal{O} be the occupied set and $\underline{d} > 0$ be the minimum distance, then the free set \mathcal{A} is defined as

$$\mathcal{A} = \{\mathbf{a} \in \mathcal{W} : \|\mathbf{a} - \mathbf{o}\|_2 \geq \underline{d} \quad \forall \mathbf{o} \in \mathcal{O}\}.$$

Remark: This definition implies that the free set \mathcal{A} and the occupied set \mathcal{O} are disjoint, i.e. $\mathcal{A} \cap \mathcal{O} = \emptyset$.

We can now formulate an obstacle avoidance constraint by enforcing that the robot's position lies within an n -dimensional ball formed around $\mathbf{c} \in \mathcal{A}$ as shown in Fig. 2.

Definition 2: For an arbitrary free point $\mathbf{c} \in \mathcal{A}$ we define the *free ball* as $\mathcal{A}_{\mathbf{c}} := \{\mathbf{p} \in \mathcal{W} : \|\mathbf{p} - \mathbf{c}\|_2 \leq d_{\mathcal{O}}(\mathbf{c}) - \underline{d}\}$. We will now show that a free ball is a convex subset of the free set.

Lemma 2: Let $\mathbf{c} \in \mathcal{A}$ be a free point, then the free ball $\mathcal{A}_{\mathbf{c}}$ is a convex subset of \mathcal{A} , i.e. $\mathbf{c} \in \mathcal{A} \Rightarrow \mathcal{A}_{\mathbf{c}} \subseteq \mathcal{A}$.

Proof: We will prove this lemma in two steps. First, we observe that the free ball is a norm ball and therefore convex. Second, we prove the lemma by contradiction, i.e. we prove $\mathcal{A}_{\mathbf{c}} \not\subseteq \mathcal{A} \Rightarrow \mathbf{c} \notin \mathcal{A}$.

Suppose $\exists \mathbf{o} \in \mathcal{O}$ and $\mathbf{p} \in \mathcal{A}_{\mathbf{c}}$ such that $\|\mathbf{p} - \mathbf{o}\|_2 < \underline{d}$. We now apply the triangle inequality and obtain $\|\mathbf{c} - \mathbf{o}\|_2 \leq \|\mathbf{p} - \mathbf{c}\|_2 + \|\mathbf{p} - \mathbf{o}\|_2 < \|\mathbf{p} - \mathbf{c}\|_2 + \underline{d}$, see Fig. 2b. Using the distance function's definition we get $d_{\mathcal{O}}(\mathbf{c}) < \|\mathbf{p} - \mathbf{c}\|_2 + \underline{d}$. Reordering yields $\|\mathbf{p} - \mathbf{c}\|_2 > d_{\mathcal{O}}(\mathbf{c}) - \underline{d}$, which shows that $\mathbf{p} \notin \mathcal{A}_{\mathbf{c}}$. ■

Based on Lem. 2 and Def. 2 we can approximate the collision avoidance constraint by $\|\mathbf{p} - \mathbf{c}\|_2 \leq d_{\mathcal{O}}(\mathbf{c}) - \underline{d}$, which is not differentiable in $\mathbf{p} = \mathbf{c}$ and might pose a problem for gradient based solvers. To circumvent this problem we square both sides of the inequality which gives us

$$\|\mathbf{p} - \mathbf{c}\|_2^2 \leq (d_{\mathcal{O}}(\mathbf{c}) - \underline{d})^2 \quad (4)$$

This transformation is only valid if both sides of the original inequality are greater or equal to 0. For the left side this is clearly given, the right hand side however becomes smaller than 0 for not-free $\mathbf{c} \notin \mathcal{A}$. To prevent this case and linear independence constraint qualification (LICQ) violations at the only feasible point we assume $d_{\mathcal{O}}(\mathbf{c}) > \underline{d}$.

With the constraint formulated in (4) and assuming that LICQ holds for all free ball center points \mathbf{c}_k with $k = 0, \dots, N$,

we can partially convexify the NLP (3). We obtain the CIAO-NLP, which like (3) depends on \mathbf{r} , $\bar{\mathbf{x}}_0$, Δt , and additionally the tuple of center points $\mathbf{C} = (\mathbf{c}_0, \dots, \mathbf{c}_N)$:

$$\min_{\mathbf{w}, \mathbf{s}} J(\mathbf{w}, \mathbf{r}) + \sum_{k=0}^N \mu_k \cdot s_k \quad (5a)$$

$$\text{s.t.} \quad \mathbf{x}_0 - \bar{\mathbf{x}}_0 = 0, \quad (5b)$$

$$\mathbf{x}_N \in \mathbb{X}_T, \quad (5c)$$

$$\mathbf{x}_{k+1} - F(\mathbf{x}_k, \mathbf{u}_k; \Delta t) = 0, \quad k = 0, \dots, N-1, \quad (5d)$$

$$h(\mathbf{x}_k, \mathbf{u}_k) \leq 0, \quad k = 0, \dots, N, \quad (5e)$$

$$\|\mathbf{p}_k - \mathbf{c}_k\|_2^2 \leq (d_{\mathcal{O}}(\mathbf{c}_k) - \underline{d}_k)^2 + s_k, \quad k = 0, \dots, N, \quad (5f)$$

$$s_k \geq 0, \quad k = 0, \dots, N. \quad (5g)$$

This reformulation of the actual NLP (3) is called Convex Inner AppRoximation (CIAO). For numerical stability we include slack variables $\mathbf{s} = [s_0, \dots, s_N]^\top \in \mathbb{R}^{N+1}$ that are penalized. A point is only considered admissible if all slacks are zero, i.e. $\mathbf{s} = 0$ in a vector sense. To ensure that the slacks are only active for problems, that would be infeasible otherwise, the multipliers μ_k have to be chosen sufficiently large, i.e. $\mu_k \gg 1$ for $k = 0, \dots, N$. The feasible set for optimization variables \mathbf{w} of this NLP depends on \mathbf{C} and is denoted as $\mathcal{F}_{(5)}(\mathbf{C})$, recall that $\mathbf{w} = [\mathbf{x}_0^\top, \mathbf{u}_0^\top, \dots, \mathbf{u}_{N-1}^\top, \mathbf{x}_N^\top]^\top$ and $\mathbf{p}_k = S_{\mathbf{p}} \cdot \mathbf{x}_k$.

An important feature of CIAO is that the distance function $d_{\mathcal{O}}(\mathbf{c})$ enters the NLP as a constant (\mathbf{c} is a parameter not an optimization variable). Thereby it can easily be used with any implementation of the Euclidean distance to the closest obstacle, even not differentiable ones, such as distance maps. We will now show some important properties of the CIAO-NLP.

Lemma 3: For a convex objective $J(\cdot)$, a convex terminal set \mathbb{X}_T , affine dynamics F , and convex path constraints h , the CIAO-NLP (5) is convex.

Proof: This follows directly from the definition of a convex optimization problem, cf. [24] (p. 136). ■

Lemma 4: For a linear-quadratic objective $J(\cdot)$, affine-quadratic path constraints h , affine dynamics F , and a terminal set \mathbb{X}_T that can be written as either (i) an affine equality or (ii) an affine-quadratic inequality constraint, CIAO-NLP (5) is a quadratically constrained quadratic program (QCQP). If also the assumptions of Lem. 3 hold, it is a convex QCQP.

Proof: This follows directly from the definition of a QCQP, cf. [24] (p. 152) and Lem. 3. ■

Lemma 5: Given $d_{\mathcal{O}}(\mathbf{c}) > \underline{d} \forall \mathbf{c} \in \mathbf{C} \Rightarrow \mathcal{F}_{(5)}(\mathbf{C}) \subseteq \mathcal{F}_{(3)}$, i.e. each feasible point of the CIAO-NLP (5) is a feasible point of the original NLP (3).

Proof: We observe that (3) and (5) are identical except for the collision avoidance constraint (3f) and (5f). As stated above $\mathbf{s} = 0$ holds for feasible points, thus the slacks \mathbf{s} can be ignored. As shown in Lem. 2 (5f) is a convex inner approximation of (3f), therefore $\mathcal{F}_{(5)}(\mathbf{C}) \subseteq \mathcal{F}_{(3)}$ follows by construction. ■

B. The CIAO-iteration

We will now introduce the CIAO-iteration, as detailed in Alg. 1. It takes a two step approach that first formulates

Algorithm 1 the CIAO-iteration

```

1: function CIAO-ITERATION( $\mathbf{w}; \mathbf{r}, \bar{\mathbf{x}}_0, \Delta t$ )
2:    $\mathbf{C} \leftarrow (\mathbf{c}_k = S_{\mathbf{p}} \cdot \mathbf{x}_k \text{ for } k = 0, \dots, N)$   $\triangleright$  recall  $\mathbf{x}_k \in \mathbf{w}$ 
3:    $\mathbf{C}^* \leftarrow (\mathbf{c}^* = \text{MAXIMIZEFB}(\mathbf{c}) \text{ for all } \mathbf{c} \in \mathbf{C})$   $\triangleright$  solve (6)
4:    $\mathbf{w}^* \leftarrow \text{SOLVENLP}(\mathbf{w}; \mathbf{C}^*, \mathbf{r}, \bar{\mathbf{x}}_0, \Delta t)$   $\triangleright$  solve (5)
5: end function return  $\mathbf{w}^*$   $\triangleright$  return newly found trajectory

```

the CIAO-NLP (5) by finding a tuple of center points $\mathbf{C} = (\mathbf{c}_0, \dots, \mathbf{c}_N)$ before solving it.

In Line 2 we find an initial tuple of center points \mathbf{C} . In practice the free balls resulting from these center points are very small and therefore very restrictive, which leaves little room for optimization, especially if the initial guess \mathbf{w} approaches obstacles closely. To overcome this problem we maximize free balls (FBs) (Line 3) by solving the following optimization problem for each $\mathbf{c} \in \mathbf{C}$ and obtain an optimized center point $\mathbf{c}^* = \eta \cdot \mathbf{g} + \mathbf{c}$:

$$\max_{\eta \geq 0} \eta \quad \text{s.t.} \quad d_{\mathcal{O}}(\eta \cdot \mathbf{g} + \mathbf{c}) = \eta + d_{\mathcal{O}}(\mathbf{c}), \quad (6)$$

where $\mathbf{c} \in \mathcal{A}$ is a given initial point, $\mathbf{g} \in \mathbb{R}^n$ is the search direction with $\|\mathbf{g}\|_2 = 1$ and η is the step size. It yields a maximized free ball $\mathcal{A}_{\mathbf{c}^*}$ with radius $r = d_{\mathcal{O}}(\mathbf{c}^*)$ with center point $\mathbf{c}^* = \eta \cdot \mathbf{g} + \mathbf{c}$ for each $\mathbf{c} \in \mathbf{C}$. The optimized center points are collected in the tuple $\mathbf{C}^* = (\mathbf{c}_0^*, \dots, \mathbf{c}_N^*)$.

We will now show that the optimization problem (6) preserves feasibility of the initial guess \mathbf{w} by showing that $\mathcal{A}_{\mathbf{c}^*}$ includes $\mathcal{A}_{\mathbf{c}}$, i.e. $\mathcal{A}_{\mathbf{c}} \subseteq \mathcal{A}_{\mathbf{c}^*}$.

Lemma 6: For $\mathbf{c} \in \mathcal{A}$, $\mathbf{g} \in \{g \in \mathbb{R}^n : \|g\|_2 = 1\}$ and $\eta \geq 0$, $d_{\mathcal{O}}(\mathbf{c}^*) = \eta + d_{\mathcal{O}}(\mathbf{c}) \Rightarrow \mathcal{A}_{\mathbf{c}} \subseteq \mathcal{A}_{\mathbf{c}^*}$ holds with $\mathbf{c}^* = \eta \cdot \mathbf{g} + \mathbf{c}$.

Proof: We will prove this by contradiction, assuming $\exists \mathbf{p} \in \mathcal{A}_{\mathbf{c}}$ s.t. $\mathbf{p} \notin \mathcal{A}_{\mathbf{c}^*}$. Using Def. 2 we can rewrite this as $\|(\eta \cdot \mathbf{g} + \mathbf{c}) - \mathbf{p}\|_2 > d_{\mathcal{O}}(\mathbf{c}^*) - \underline{d}$. Applying the triangle inequality on the left side yields $\|\mathbf{p} - (\mathbf{c} + \eta \cdot \mathbf{g})\|_2 \leq \|\mathbf{p} - \mathbf{c}\|_2 + \|\eta \cdot \mathbf{g}\|_2 = \|\mathbf{p} - \mathbf{c}\|_2 + \eta$ and based on our assumption $\|\mathbf{p} - \mathbf{c}\|_2 + \eta \leq d_{\mathcal{O}}(\mathbf{c}) - \underline{d} + \eta$ holds. Inserting this gives $d_{\mathcal{O}}(\mathbf{c}) + \eta - \underline{d} > d_{\mathcal{O}}(\mathbf{c}^*) - \underline{d}$ and thus contradicts the condition $d_{\mathcal{O}}(\mathbf{c}^*) = \eta + d_{\mathcal{O}}(\mathbf{c})$. ■

To solve the line search problem (6) we propose to use the distance function's normalized gradient $\mathbf{g} = \frac{\nabla d_{\mathcal{O}}(\mathbf{c})}{\|\nabla d_{\mathcal{O}}(\mathbf{c})\|_2}$ as search direction. Starting from $\eta = \underline{\eta} > 0$ the step size is exponentially increased until a step size $\bar{\eta} > \underline{\eta}$ is found for which the constraint is violated. The optimal step size can now be found using the bisection method. SOLVENLP uses a suitable solver to solve (5), e.g. Ipopt [25], and computes a new trajectory \mathbf{w}^* (Line 4).

Lemma 7: For a feasible initial guess $\mathbf{w} \in \mathcal{F}_{(3)}$ Alg. 1 finds a feasible point $\mathbf{w}^* \in \mathcal{F}_{(3)}$ with $J(\mathbf{w}^*) \leq J(\mathbf{w})$.

Proof: We prove this in two steps: first we assume that SOLVENLP uses a suitable, working NLP-solver, then we show the feasibility. From $\mathcal{A}_{\mathbf{c}} \subseteq \mathcal{A}_{\mathbf{c}^*}$ as shown in Lem. 6 follows $\mathcal{F}_{(5)}(\mathbf{C}) \subseteq \mathcal{F}_{(5)}(\mathbf{C}^*)$. Further Lem. 5 yields $\mathcal{F}_{(5)}(\mathbf{C}) \subseteq \mathcal{F}_{(5)}(\mathbf{C}^*) \subseteq \mathcal{F}_{(3)}$. ■

C. Continuous Time Collision Avoidance for Systems with Bounded Acceleration

The constraints formulated in (4) can be extended to the continuous time case. Using Lem. 2 we can write the continuous time collision avoidance constraint as

$$\|\mathbf{c}_k - \mathbf{p}(t)\|_2 \leq d_{\mathcal{O}}(\mathbf{c}_k) - \underline{d} \quad \forall t \in [t_k, t_{k+1}], k = 0, \dots, N.$$

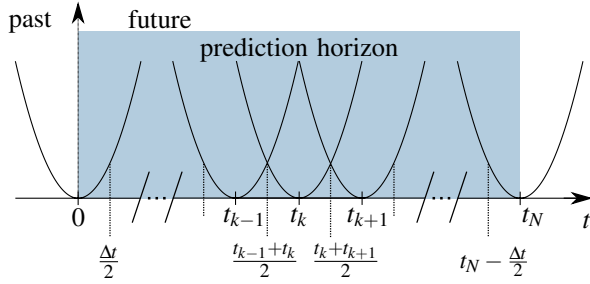


Fig. 3: Maximal action radius between sampling points.

Assuming a double integrator model of the form $\mathbf{p}(t) = \mathbf{p}_k + \dot{\mathbf{p}}_k \cdot (t - t_k) + \int_{t_k}^t \int_{t_k}^{\tau} \ddot{\mathbf{p}}(s) ds d\tau$ with the shorthand $\mathbf{p}_k = \mathbf{p}(t_k)$ for all $k = 0, \dots, N$ with $t \in [t_k, t_{k+1}]$ it can be written as

$$\left\| \mathbf{p}_k + \dot{\mathbf{p}}_k \cdot (t - t_k) + \int_{t_k}^t \int_{t_k}^{\tau} \ddot{\mathbf{p}}(s) ds d\tau - \mathbf{c}_k \right\|_2 \leq d_{\mathcal{O}}(\mathbf{c}_k) - \underline{d}.$$

Using the triangle inequality we get

$$\|\mathbf{p}_k - \mathbf{c}_k\|_2 \leq d_{\mathcal{O}}(\mathbf{c}_k) - \underline{d} - \|\dot{\mathbf{p}}_k\|_2 \cdot (t - t_k) - \left\| \int_{t_k}^t \int_{t_k}^{\tau} \ddot{\mathbf{p}}(s) ds d\tau \right\|_2.$$

With $\|\int \ddot{\mathbf{p}}(\tau) d\tau\|_2 \leq \int \|\ddot{\mathbf{p}}(\tau)\|_2 d\tau$ and assuming that system's total acceleration is bounded $\|\ddot{\mathbf{p}}(t)\|_2 \leq \bar{a} \forall t \in \mathbb{R}$, which is a reasonable assumption for most physical systems, yields

$$\|\mathbf{p}_k - \mathbf{c}_k\|_2 \leq d_{\mathcal{O}}(\mathbf{c}_k) - \underline{d} - \|\dot{\mathbf{p}}_k\|_2 \cdot (t - t_k) - \frac{\bar{a}}{2} \cdot (t - t_k)^2.$$

We assume that velocities are bounded in all discretization points, i.e., $\|\dot{\mathbf{p}}_k\|_2 \leq \bar{v}$ for $k = 0, \dots, N$. Considering that $t_0 - \frac{\Delta t}{2}$ and $t_N + \frac{\Delta t}{2}$ lie outside of the prediction horizon and that $\|\dot{\mathbf{p}}_{k \pm 1}\|_2 \leq \bar{v}$ for $k = 1, \dots, N-1$, it is sufficient to ensure collision freedom for $t_k \pm \frac{\Delta t}{2}$ and get

$$\|\mathbf{p}_k - \mathbf{c}_k\|_2 \leq d_{\mathcal{O}}(\mathbf{c}_k) - \underline{d} - \bar{v} \cdot \frac{\Delta t}{2} - \bar{a} \cdot \frac{\Delta t^2}{8} \quad \text{for } k = 0, \dots, N.$$

To illustrate the reasoning Fig. 3 sketches the maximum deviation from the current location over time. For the sake of simplicity we assume

$$\underline{d}_k > \bar{v} \cdot \frac{\Delta t}{2} + \bar{a} \cdot \frac{\Delta t^2}{8} \quad k = 0, 1, \dots, N \quad (7)$$

from now on, such that (5f) guarantees continuous-time collision freedom is under the assumptions made above.

Please note that by construction (7) implies that $\mathcal{A}_{\mathbf{c}_k}$ and $\mathcal{A}_{\mathbf{c}_{k+1}}$ for $k = 0, \dots, N-1$ overlap or touch in the point where the trajectory transits from one into the other.

D. Rotational Invariance Trick

Several wheeled mobile robots have a configuration space which is $SE(2)$ or $SE(3)$ and are modeled using Euler-angles. To maintain simplicity of dynamic equations and a consistency between orientation change and rotational velocity, i.e. $\theta_{k+1} = \theta_k + \int_{t_k}^{t_{k+1}} \omega dt$, where θ is robot's orientation and ω its rotational velocity, we use a continuous variable to model orientation, i.e. $\theta \in \mathbb{R}^n$. To cope with the ambitiousness of this representation we use, what we call the 'rotational invariance trick':

$$d(\theta_1, \theta_2) = \left\| \begin{bmatrix} \cos \theta_1 - \cos \theta_2 \\ \sin \theta_1 - \sin \theta_2 \end{bmatrix} \right\|_2 \quad (8)$$

which is a measure for the difference between θ_1 and θ_2 .

E. Choosing the Objective Function

In this work we consider a quadratic cost function for reference tracking with regulation:

$$J(\mathbf{w}) = \sum_{k=0}^{N-1} \alpha^k \|\mathbf{q}(\mathbf{x}_k) - \mathbf{q}(\hat{\mathbf{x}}_k)\|_Q^2 + \|\mathbf{u}_k - \hat{\mathbf{u}}_k\|_R^2 + \alpha^N \|\mathbf{q}(\mathbf{x}_N) - \mathbf{q}(\hat{\mathbf{x}}_N)\|_{Q_N}^2,$$

where $\alpha > 1$ leads to exponentially increasing stage cost and reduces oscillating behavior around the goal, $\hat{\mathbf{x}}_k, \hat{\mathbf{u}}_k$ denote reference state and controls at stage k , $\mathbf{q}: \mathbb{R}^{n_x} \rightarrow \mathbb{R}^{n_q}$ augments the state \mathbf{x} by applying the rotational invariance trick (8) where applicable, $Q, Q_N \in \mathbb{R}^{n_q \times n_q}$, and $R \in \mathbb{R}^{n_u \times n_u}$ are positive definite matrices.

V. CIAO-BASED MOTION PLANNING

In this section we propose and detail two methods, one for pure trajectory optimization and the other for simultaneous trajectory optimization and tracking by solving (5). The first method as summarized in Alg. 2 is referred to as *offline-mode*, because it requires an additional trajectory tracker to close the feedback loop online. The latter method, summarized in Alg. 3, is an *online* feedback controller. Both algorithms start by generating a feasible initial guess and a reference trajectory to follow, in each iteration free balls are computed and before their CIAO-NLP (5) is solved to compute a new trajectory that is guaranteed to be kinodynamically feasible and collision free.

A. CIAO for Trajectory Optimization

For the offline mode, the terminal constraint in (5) becomes an equality constraint, which enforces that the goal state \mathbf{x}_G is reached at the end of the horizon, i.e. $\mathbb{X}_T = \{\mathbf{x}_G\}$.

Algorithm 2 CIAO for offline trajectory optimization

Require: $\mathbf{x}_S, \mathbf{x}_G, \Delta t, \varepsilon$ ▷ start and goal state
1: $\mathbf{w}^* \leftarrow \text{INITIALGUESS}(\mathbf{x}_S, \mathbf{x}_G, \Delta t)$ ▷ feasible initialization
2: $\mathbf{r} \leftarrow \text{REFERENCETRAJECTORY}(\mathbf{x}_S, \mathbf{x}_G, \Delta t)$
3: **do**
4: $\mathbf{w} \leftarrow \mathbf{w}^*$ ▷ set last solution as initial guess
5: $\mathbf{w}^* \leftarrow \text{CIAO-ITERATION}(\mathbf{w}; \mathbf{r}, \bar{\mathbf{x}}_0, \Delta t)$ ▷ $\bar{\mathbf{x}}_0 = \mathbf{x}_S$
6: **while** $\text{COST}(\mathbf{w}^*) - \text{COST}(\mathbf{w}) > \varepsilon$
7: **return** \mathbf{w}^*

The algorithms starts by computing a feasible initial guess and a reference trajectory (Lines 1–2). In the general case of nonconvex scenarios, such as cluttered environments, feasible initializations can be obtained through a sampling-based motion planner. To monitor the progress the initial guess is copied (Line 4), before using it as initial guess for the CIAO-ITERATION (Line 5). Lines 4–5 are repeated as long as the COST-function shows an improvement that exceeds a given threshold ε (Line 6). Finally best known solution \mathbf{w}^* is returned (Line 7).

B. CIAO-NMPC

While Alg. 2 iteratively improves a trajectory that connects \mathbf{x}_S and \mathbf{x}_G , Alg. 3 uses a shorter, receding horizon. This can be considered the real-time iteration (RTI) version of Alg. 2. Therefore the trajectory computed by INITIALGUESS (Line 1) is not required to reach the goal state $\mathbf{x}_G \in \mathbb{X}_G$. In

Algorithm 3 CIAO-NMPC

Require: $\bar{\mathbf{x}}_0, \mathbf{x}_G, \Delta t, \mathbb{X}_G$ \triangleright current and goal state
1: $\mathbf{w} \leftarrow \text{INITIALGUESS}(\bar{\mathbf{x}}_0, \mathbf{x}_G, \Delta t)$ \triangleright feasible initialization
2: **while** $\bar{\mathbf{x}}_0 \notin \mathbb{X}_G$ **do**
3: $\bar{\mathbf{x}}_0 \leftarrow \text{GETCURRENTSTATE}()$
4: $\mathbf{r} \leftarrow \text{REFERENCETRAJECTORY}(\bar{\mathbf{x}}_0, \mathbf{x}_G, \Delta t)$
5: $\mathbf{w}^* \leftarrow \text{CIAO-ITERATION}(\mathbf{w}; \mathbf{r}, \bar{\mathbf{x}}_0, \Delta t)$ \triangleright Alg. 1
6: $\text{APPLYFIRSTCONTROL}(\mathbf{w}^*)$ \triangleright recall $\mathbf{u}_0 \in \mathbf{w}^*$
7: $\mathbf{w} \leftarrow \text{SHIFTTTRAJECTORY}(\mathbf{w}^*)$ \triangleright recede horizon
8: **end while**

may cases it is sufficient to choose $\mathbf{w} = [\mathbf{x}_0^\top, \mathbf{u}_s^\top, \dots, \mathbf{u}_s^\top, \mathbf{x}_0^\top]^\top$, where \mathbf{u}_s is chosen, such that the robot remains in the current state \mathbf{x}_0 . While the robot has not reached the goal region \mathbb{X}_G (Line 2), it is iteratively steered to it (Lines 3–8). Each iteration starts by updating the robot’s current state \mathbf{x}_0 . Based on the complexity of the scenario $\text{REFERENCETRAJECTORY}$ may return a guiding trajectory to the goal or just the goal state itself (Line 4). We run Alg. 1 to compute a new trajectory (Line 5), before sending the first control to the robot (Line 6). SHIFTTTRAJECTORY moves the horizon one step forward (Line 7).

To ensure collision freedom, the terminal constraint (5c) is commonly chosen such that the robot comes to a full stop at the end of the horizon, i.e. $\mathbb{X}_T = \{\mathbf{x} \in \mathbb{R}^{n_x} : S_v \cdot \mathbf{x} = \mathbf{0}\}$, where $S_v \in \mathbb{R}^{n_v \times n_x}$ is the matrix that selects the velocities from the state vector.

VI. EXPERIMENTS AND DISCUSSION

To evaluate CIAO in terms of planning efficiency and final path quality, we compare it against a set of baselines. We challenge CIAO by breaking a few assumptions made above. Namely we consider nonlinear dynamics, use a nonconvex cost function, due to the rotational invariance trick, and initialize it with a collision free path that does not satisfy the robot’s dynamics. In this case interior point NLP-solvers are well suited and can handle nonlinear convex constraints efficiently. For this reason, we use Ipopt [26] with the linear solver MA-27 [27] called through CasADi [28] (version 3.4.5) to solve CIAO-NLPs (5) in all experiments.

For the evaluation, we design three types of experiments: (A) numerical experiments to investigate the behavior of the free ball constraint against competing formulations; (B) a trajectory optimization benchmark; (C) real-world experiments where CIAO is qualitatively compared to a state of the art baseline.

A. Comparison of constraint formulations

In a first set of experiments the numerical performance of the free ball constraint formulation as derived in Sec. IV-A is compared to common alternatives: the actual constraint as defined in Lem. 1 (actual), a linearization of the actual constraint (linear), and a log-barrier formulation (log-barrier). They differ only in the way the obstacle avoidance constraint (3f) is formulated. Our findings are reported in Tab. I.

The average computation time taken per MPC-step and per Ipopt iteration are given as ‘ms / step’ and ‘ms / iteration’ respectively, ‘iters / step’ are the average Ipopt iterations per MPC-step. The path quality is evaluated in terms of ‘time to goal’ and ‘path length’. Averages in the first five rows are

	<i>actual</i>	<i>linear</i>	<i>CIAO</i>	<i>log-barrier</i>
ms / iteration	2.00	0.72	0.70	2.23
ms / step	40.78	13.13	17.26	50.34
iterations / step	20.35	18.23	24.64	22.57
time to goal [s]	14.35	14.39	18.67	(13.46)*
path length [m]	10.22	10.33	10.58	(9.25)*
max ms / step	448.94	230.07	179.26	> 1000
% timeouts	0	0	0	11.3

TABLE I: Comparison of constraint formulations.¹

taken over 62 scenarios, for which the maximum CPU time of 1.0s was not exceeded. The percentage of runs that exceed the CPU time is given by ‘% timeouts’. The maximum CPU time required for a single MPC-step is given by ‘max ms / step’.

We observe that the actual constraint is producing both fastest and shortest paths. This path quality comes at comparatively high computational cost. Linearizing the actual constraint reduces the computational effort while maintaining a high path quality. In contrast to CIAO, linearization is not an inner approximation and can lead to constraint violations that necessitate computationally expensive recovery iterations. This increases the over all computation time significantly and leads to a higher maximal computation time. At the cost of lower path quality, but a similar average computation time, CIAO overcomes this problem by preserving feasibility. This leads to a lower variance in the computation time, and allows for collision freedom guarantees. A further advantage, which is relevant in practice, is that CIAO generalizes to not continuously differentiable distance function implementations, e.g. distance fields.

Including the collision avoidance constraint as a barrier term in the objective, i.e. by adding $-\log(d_\sigma(p_k) - \underline{d})$ to the stage cost l_k , is an alternative approach to enforce collision freedom. Our results suggest, however, that for our application is least favorable among the considered options.

B. Trajectory Optimization Benchmark

In a second set of experiments CIAO is compared to GuSTO [6] using the implementation publicly provided by the authors. In these experiments we consider a 3-D Astrobbee Robot with 12 states and 6 controls, that has to be brought from a start position on the left of a $10 \times 10 \times 10$ m cube to a goal right. The room between start and goal point is cluttered with 25 randomly placed static obstacles of varying sizes (between 1 and 2 meters). Fig. 1 shows some examples.

The results reported in Tab. II and Fig. 4 were in Julia on a MacBook Pro with an Intel Core i7-8559U clocked at 2.7GHz. The SCPs formulated by GuSTO [6] are solved with Gurobi [29]. Both algorithms are provided with the same initial guess, which is computed based on a path found with RRT [30]. We used a horizon of 100 s initially equally split into 250 steps, resulting in a sampling time of 0.4 s.

¹These experiments were conducted in simulation considering a robot with differential drive dynamics (5 states, 2 controls) and a prediction horizon of 50 steps, resulting in a total of 405 optimization variables.

* not representative because complex scenarios with long transitions failed.

²These timings are only indicative due to differences in implementation, a similar trend is confirmed in Fig. 6.

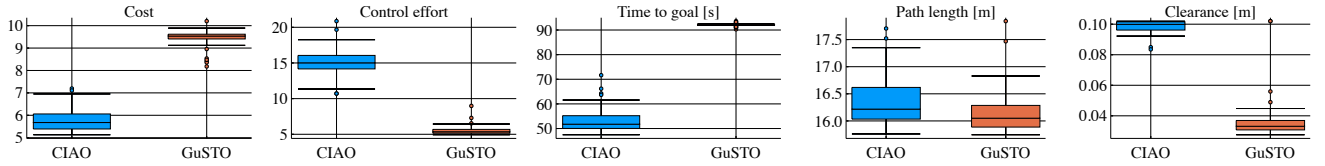


Fig. 4: Trajectory Optimization Benchmark Results

measure	CIAO	GuSTO
Compute ² [s]	14.792±11.966	131.367±130.743
Iterations	30.660±15.886	4.520±1.282
Compute / Iteration [s]	0.475±0.230	27.729±22.096
Linearization Error	4.66e-14±3.67e-15	4.10e-06±1.28e-06

TABLE II: Numerical Performance: Average \pm std values.

In our experiments both CIAO and GuSTO find solutions to all considered scenarios. As reported in Tab. II CIAO (Alg. 2) requires more iterations to converge but the individual iterations are cheaper. An important difference between the algorithms is that CIAO obtains a feasible trajectory after the first iteration and therefore could be terminated early, while GuSTO does not have this property and takes several iterations to find a feasible trajectory. Even though the dynamics are mostly linear we observe linearization errors for GuSTO, originating from the linear model they use.

Since both GuSTO and CIAO use tailored cost functions we evaluate the computed trajectories using a common cost function J_ρ which is based on the state distance metric $\rho: R^{n_x} \times R^{n_x} \rightarrow \mathbb{R}$ proposed by [31]: $J_\rho(\mathbf{w}; \mathbf{x}_G) = \sum_{k=0}^N \rho(\mathbf{x}_k, \mathbf{x}_G)$, with goal state \mathbf{x}_G and all weights of the distance metric chosen equal. We observe, that CIAO achieves significantly lower cost, because it reaches the goal faster. The controls are evaluated separately and reported as control effort given by $J_u(\mathbf{w}) = \sum_{k=0}^{N-1} \Delta t \cdot \|\mathbf{u}_k\|_1$. The path quality is evaluated in terms of time to goal, path length, and clearance (minimum distance to the closest obstacle along the trajectory). The first two measure to the time and path length until the state distance metric is below a threshold of 0.5, while the latter one is evaluated on the entire trajectory. These three metrics are evaluated on an oversampled trajectory using a sampling time $\Delta t = 0.01$ s.

Compared to GuSTO, CIAO finds slightly longer paths because it maintains a higher clearance. This behavior allows for a higher average speed, at the cost of the highest control among the compared methods and leads to shorter times to goal. Representative examples are shown in Fig. 1.

C. Real-World Experiments - Differential Drive Robot

To qualitatively assess the behavior of CIAO-NMPC (Alg. 3) it was tested in dynamic real-world scenarios with freely moving humans. A representative example is depicted in Fig. 5. Note that CIAO has no knowledge of the humans' future movements. It is instead considering all humans as static obstacles in their current position.

As in Sec. VI-A a differential drive robot is used, this time with a horizon of 5s and a control frequency of 10 Hz resulting in a total of 405 optimization variables (including slacks). For these experiments CIAO was implemented as

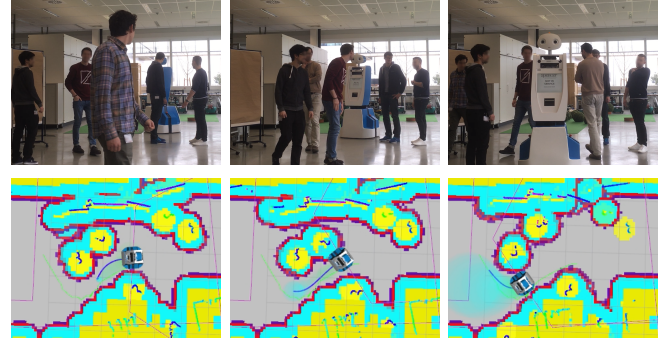


Fig. 5: CIAO steers a wheeled mobile robot through a group of people. Real-world (top) and RViz (bottom): Planned trajectory as blue line, free balls as transparent circles, obstacles in yellow, safety margin in light blue.

a C++ ROS-module, the distance function was realized as distance field based on the code by [32]. Initial guesses and reference paths were computed using an A* algorithm [33].

Since GuSTO is not suitable for receding horizon control (RHC), we used an extended version of the elastic-band method [13]. To obtain comparable results, we used the same global planner and localization method with both algorithms. The people were allowed to move freely and react to the robot's behavior at their own choosing, while leaving only small passages for the robot, as shown in the top of Fig. 5.

In Fig. 5, it can be seen that the free balls (FBs) (transparent circles) keep to the center of the canyon-like free space. The predicted trajectory (blue line) is deformed to stay inside the FBs. This is a predictive adaptation to the changed environment. For the shown, representative example in Fig. 5 the robot passed smoothly the group. The elastic-band approach solved comparable scenarios similarly.

Groups of people pose a particular challenge that could, however, be solved by both approaches. We note that the robot is moving a bit faster in proximity to people for the elastic-band approach, while our method adjusts to blocked paths a bit faster. The most significant difference between the methods is that CIAO combines rotation and backward/forward motion, while the elastic-band method turns the robot on the spot. Both methods succeeded in steering the robot through the group safely, without a single collision.

Fig. 6 shows representative computation times obtained in simulation on a set of 14 scenarios involving non-deterministically moving virtual humans. The reported computation time accounts only for solving the CIAO-NLP and function evaluations in CasADi, the processing time required by preprocessing steps and other components is not included. High computation times originate from far-from-optimal initializations occurring when a new goal is set, i.e.

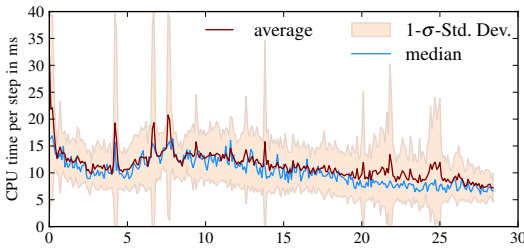


Fig. 6: NLP-solver times obtained in a simulated environment including non-deterministically moving humans. A comparison of these computation times with the ones reported in [6] indicates, that CIAO is computationally cheaper than GuSTO.

around time $t = 0$, or if humans cross the planned path.

VII. CONCLUSIONS AND FUTURE WORK

This work proposes CIAO, a new framework for trajectory optimization, that is based on a novel constraint formulation. It uses a multiple-shooting scheme and can be solved efficiently by an interior point solver. We show that it reaches or exceeds state of the art performance in trajectory optimization at significantly lower computational effort, scales to high dimensional systems, and that it can be used for RHC style MPC of mobile robots in dynamic environments. To the authors' knowledge this is the first work that uses constrained optimization for unified trajectory optimization and control. The experiments show that method scales to high dimensional robots.

Future research will focus on extending CIAO to full body collision checking, guaranteed obstacle avoidance in dynamic environments, and time optimal motion planning. A second focus will lie on efficient numerical methods that exploit CIAO's properties shown in Lem. 3 and 4.

ACKNOWLEDGMENTS

This work has received funding from the EUs Horizon 2020 research and innovation program under grant agreement No 732737 (ILIAD).

REFERENCES

- [1] D. Verscheure, B. Demeulenaere, J. Swevers, J. D. Schutter, and M. Diehl, "Time-optimal path tracking for robots: a convex optimization approach," *IEEE Trans. Autom. Control*, vol. 54, pp. 2318–2327, 2009.
- [2] M. Zucker, N. Ratliff, A. D. Dragan, M. Pivtoraiko, M. Klingensmith, C. M. Dellin, J. A. Bagnell, and S. S. Srinivasa, "CHOMP: Covariant Hamiltonian Optimization for Motion Planning," *Int. J. Rob. Res.*, vol. 32, no. 9–10, pp. 1164–1193, 2013.
- [3] J. Schulman, Y. Duan, J. Ho, A. Lee, I. Awwal, H. Bradlow, J. Pan, S. Patil, K. Goldberg, and P. Abbeel, "Motion planning with sequential convex optimization and convex collision checking," *Int. J. Rob. Res.*, vol. 33, no. 9, pp. 1251–1270, 2014.
- [4] S. L. Herbert, M. Chen, S. Han, S. Bansal, J. F. Fisac, and C. J. Tomlin, "FaSTrack: a modular framework for fast and guaranteed safe motion planning," in *IEEE Conf. Decis. Control (CDC)*, 2017, pp. 1517–1522.
- [5] X. Zhang, A. Liniger, and F. Borrelli, "Optimization-based collision avoidance," *arXiv preprint arXiv:1711.03449*, 2017.
- [6] R. Bonalli, A. Cauligi, A. Bylard, and M. Pavone, "GuSTO: Guaranteed Sequential Trajectory Optimization via sequential convex programming," in *IEEE Int. Conf. Rob. Autom. (ICRA)*, 2019.
- [7] Z. Zhu, E. Schmerling, and M. Pavone, "A convex optimization approach to smooth trajectories for motion planning with car-like robots," in *IEEE Conf. Decis. Control (CDC)*, 2015, pp. 835–842.

- [8] J. V. Frasca, A. J. Gray, M. Zanon, H. J. Ferreau, S. Sager, F. Borrelli, and M. Diehl, "An auto-generated nonlinear MPC algorithm for real-time obstacle avoidance of ground vehicles," in *Eur. Control Conf. (ECC)*, 2013, pp. 4136–4141.
- [9] A. Liniger, A. Domahidi, and M. Morari, "Optimization-based autonomous racing of 1:43 scale RC cars," *Optimal Control Applications and Methods*, vol. 36, no. 5, pp. 628–647, 2015.
- [10] T. Faulwasser and R. Findeisen, "Nonlinear model predictive control for constrained output path following," *IEEE Trans. Autom. Control*, vol. 61, no. 4, pp. 1026–1039, 2016.
- [11] M. Neunert, C. de Crousaz, F. Furrer, M. Kamel, F. Farshidian, R. Siegwart, and J. Buchli, "Fast nonlinear model predictive control for unified trajectory optimization and tracking," in *IEEE Int. Conf. Rob. Autom. (ICRA)*, 2016, pp. 1398–1404.
- [12] S. Karaman and E. Frazzoli, "Sampling-based algorithms for optimal motion planning," *Int. J. Rob. Res.*, vol. 30, no. 7, pp. 846–894, 2011.
- [13] S. Quinlan and O. Khatib, "Elastic bands: Connecting path planning and control," in *IEEE Int. Conf. Rob. Autom. (ICRA)*, vol. 2, 1993, pp. 802–807.
- [14] O. Brock and O. Khatib, "Elastic strips: A framework for motion generation in human environments," *Int. J. Rob. Res.*, vol. 21, no. 12, pp. 1031–1052, 2002.
- [15] D. Kouzoupis, G. Frison, A. Zanelli, and M. Diehl, "Recent advances in quadratic programming algorithms for nonlinear model predictive control," *Vietnam J. of Math.*, vol. 46, no. 4, pp. 863–882, 2018.
- [16] H. G. Bock and K. J. Plitt, "A multiple shooting algorithm for direct solution of optimal control problems," in *Proceedings of the IFAC World Congress*. Pergamon Press, 1984, pp. 242–247.
- [17] C. Rösmann, F. Hoffmann, and T. Bertram, "Integrated online trajectory planning and optimization in distinctive topologies," *Robotics and Autonomous Systems*, vol. 88, pp. 142–153, 2017.
- [18] J. Borenstein and Y. Koren, "The vector field histogram – fast obstacle avoidance for mobile robots," *IEEE Trans. Rob. Autom.*, vol. 7, no. 3, pp. 278 – 288, 1991.
- [19] D. Fox, W. Burgard, and S. Thrun, "The dynamic window approach to collision avoidance," *IEEE Rob. Autom. Mag.*, vol. 4, no. 1, pp. 23 – 33, 1997.
- [20] N. Y. Ko and R. G. Simmons, "The lane-curvature method for local obstacle avoidance," in *IEEE/RSJ Int. Conf. Intell. Rob. Syst. (IROS)*, vol. 3, 1998, pp. 1615 –1621.
- [21] P. Fiorini and Z. Shiller, "Motion planning in dynamic environments using velocity obstacles," *Int. J. Rob. Res.*, vol. 17, no. 7, pp. 760–772, 1998.
- [22] J. Minguez and L. Montano, "Nearness diagram (nd) navigation: Collision avoidance in troublesome scenarios," *IEEE Transactions on Robotics and Automation*, vol. 20, no. 1, pp. 45–59, February 2004.
- [23] Y. Xiang Yuan, "Recent advances in trust region algorithms," *Mathematical Programming*, vol. 151, no. 1, pp. 249–281, June 2015.
- [24] S. Boyd and L. Vandenberghe, *Convex Optimization*. Cambridge Univ. Press, 2004.
- [25] A. Wächter and L. T. Biegler, "On the implementation of an interior-point filter line-search algorithm for large-scale nonlinear programming," *Mathematical Programming*, vol. 106, no. 1, pp. 25–57, 2006.
- [26] A. Wächter and L. Biegler, "IPOPT - an Interior Point OPTimizer," <https://projects.coin-or.org/Ipopt>, 2009.
- [27] HSL, "A collection of Fortran codes for large scale scientific computation." <http://www.hsl.rl.ac.uk>, 2011.
- [28] J. A. E. Andersson, J. Gillis, G. Horn, J. B. Rawlings, and M. Diehl, "CasADi: a software framework for nonlinear optimization and optimal control," *Mathematical Programming Computation*, 2018.
- [29] Gurobi Optimization, LLC, "Gurobi optimizer reference manual."
- [30] S. M. LaValle, *Planning Algorithms*. Cambridge Univ. Press, 2006.
- [31] S. M. LaValle and J. James J. Kuffner, "Randomized kinodynamic planning," *Int. J. Rob. Res.*, vol. 20, no. 5, pp. 378–400, 2001.
- [32] B. Lau, C. Sprunk, and W. Burgard, "Efficient grid-based spatial representations for robot navigation in dynamic environments," *Robotics and Autonomous Systems*, vol. 61, no. 10, pp. 1116–1130, 2013.
- [33] P. E. Hart, N. J. Nilsson, and B. Raphael, "A formal basis for the heuristic determination of minimum cost paths," *IEEE Transactions on Systems Science and Cybernetics*, vol. 4, no. 2, pp. 100–107, 1968.